A HANDHELD OPEN-FIELD INFANT KERATOMETER (AN AMERICAN OPHTHALMOLOGICAL SOCIETY THESIS)

BY Joseph M. Miller MD MPH

ABSTRACT

Purpose: To design and evaluate a new infant keratometer that incorporates an unobstructed view of the infant with both eyes (open-field design).

Methods: The design of the open-field infant keratometer is presented, and details of its construction are given. The design incorporates a single-ring keratoscope for measurement of corneal astigmatism over a 4-mm region of the cornea and includes a rectangular grid target concentric within the ring to allow for the study of higher-order aberrations of the eye. In order to calibrate the lens and imaging system, a novel telecentric test object was constructed and used. The system was bench calibrated against steel ball bearings of known dimensions and evaluated for accuracy while being used in handheld mode in a group of 16 adult cooperative subjects. It was then evaluated for testability in a group of 10 infants and toddlers.

Results: Results indicate that while the device achieved the goal of creating an open-field instrument containing a single-ring keratoscope with a concentric grid array for the study of higher-order aberrations, additional work is required to establish better control of the vertex distance.

Conclusion: The handheld open-field infant keratometer demonstrates testability suitable for the study of infant corneal astigmatism. Use of collimated light sources in future iterations of the design must be incorporated in order to achieve the accuracy required for clinical investigation.
Trans Am Ophthalmol Soc 2010;108:77-95

INTRODUCTION

Infants are commonly found to have astigmatism, although the presence of this astigmatism has only relatively recently been recognized.[1] Uncorrected astigmatism can result in differential blur on the retina, which can lead to orientation-specific defects in vision, a type of amblyopia known as meridional amblyopia. The study of meridional amblyopia, as well as the prevention and treatment of amblyopia through spectacle wear, has been the topic of a multiyear partnership between the Tohono O'odham Nation and research funded by the National Eye Institute.[2]

The Tohono O'odham are a Native American tribe that has a high prevalence of corneal astigmatism. Over a third of the tribe have 3 diopters (D) or more of corneal astigmatism, and about 10% have 5 D or more.[2] While other tribes[2] have also been shown to have similar levels of astigmatism, the Tohono O'odham Nation is unique in their experience at providing screening for high refractive error early in childhood, and offering a comprehensive program to both supply and encourage the use of spectacles for the children of the tribe.

The astigmatism found in these children is usually corneal in origin, most often with-the-rule, and is commonly corrected for children over age 4 when more than 1.5 D of refractive astigmatism is found. The early identification of children needing astigmatic correction was found to be most readily accomplished by screening the children for refractive or corneal astigmatism using automated instruments.[3] The commercially available instruments used in the study were readily accepted by children in the Head Start age-group. Although the working distance is typically quite small (commonly 25 mm), when a trained operator was using an instrument, it was easily accepted by the children. The use of such automated instruments has been shown to greatly facilitate screening for significant refractive error.

However, as the research questions regarding astigmatism and its role in visual development began to address a target age range below 4 years, it became apparent that babies and toddlers do not take so readily to instruments that need to be held so close to the head. Pilot studies in which infants and toddlers were examined using either a handheld autorefractor or a handheld keratometer did not provide much encouragement that the use of such instruments would result in high testability.

For this reason, our research group has developed several infant keratometers through the years. The goal in developing these instruments was to provide a mechanism to measure the corneal astigmatism of an infant or toddler in a nonthreatening manner, with sufficient accuracy to characterize the astigmatism for classification but not prescribing. For example, although a quarter-diopter accuracy may be required for spectacle prescribing and even greater for planning refractive surgery, such accuracy is not needed when the goal is to classify children as having low or no astigmatism, moderate astigmatism, or high astigmatism, in order to study how the astigmatism may be affecting visual development.

COMPONENTS OF KERATOMETRY

Keratometers, also known as ophthalmometers, measure the curvature of the cornea being studied by using the tear film as a mirror. Steeply curved convex mirrors have a small radius of curvature and will form an image behind the mirror. The more steeply curved the cornea, the greater the reflecting power, and the smaller the image that is formed. The size and location of the image that is formed

From the Department of Ophthalmology and Vision Sciences, The College of Optical Sciences, and The Mel and Enid Zuckerman College of Public Health of The University of Arizona, Tucson.

are determined by three parameters: the radius of curvature of the cornea, the size of the object that is being imaged by the corneal tear film, and the distance of the object to the cornea. Conventional, mechanical keratometers present before the patient an object that is being imaged, use optical means to control the distance of that object to the subject's eye, and then either vary the size of the object to produce a fixed image size or present a fixed object and measure the image size. The Javal-Schiötz ophthalmometer operates on the former principle, and the American Optical style instruments employ the latter mechanisms.

As a class of instruments, keratometers or ophthalmometers control object distance and determine the relation of object space (arising from a point on the keratometer mire, ring, target, or point source of light) and image space (found by analysis of the corneal image of the object). Analysis of this relation between object and image, with knowledge of the object distance, allows determination of the corneal reflection power. In general, keratometers are designed to work within the central 3 mm of the cornea, where it is largely spherical.[4]

In these instruments, as knobs are turned to produce the final end state, calibration markings on the dials read out the resulting radius of curvature of the surface of the cornea and its overlying reflective tear film. Given the radius of curvature, a cornea refracting power can be estimated by dividing the keratometric index (1.3375) by the radius of curvature in meters. This keratometric index is an approximation that incorporates a small correction for the negative refracting power of the back (convex) curvature of the cornea.[5]

Object Distance

In conventional keratometers, a close-focusing telescope with very shallow depth of focus is used to control the distance from the object (illuminated light source generated a corneal reflected image) to the cornea. An operator views the subject's eye through the telescope and adjusts the apparatus until a sharply focused image is obtained. In doing so, a calibrated and known distance from the object to the subject's eye is obtained.

Object

Perhaps it is a misnomer to speak of qualitative keratometry, but the earliest keratoscopes were intended for the observer to directly inspect the corneal light reflections and to make qualitative judgments as to the presence of astigmatism. Placido's disc is an early example of such an object.

Various objects have been used for quantitative keratometry. The earliest keratometers differed significantly in the object used for corneal image formation. Placido[6] had rings, Helmholz[7] had a fixed-size object, and Javal and Schiötz[8] had a variable-sized object. A distorted checkerboard[9] has been used, which, when imaged by the cornea, demonstrates a regular grid pattern in the reflected image.

The keratometer of Helmholz introduced variable doubling in order to measure a difference in magnification. Javal and Schiötz used a pair of dissimilar objects whose angular separation could be varied, until a known image size resulted. Placido did not use quantitative methods to evaluate the reflected image, but incorporated a series of rings, or mires, that caused an illumination to occur.

Modern keratometers (as opposed to corneal topographers, as described below), which measure the corneal curvature in the central 4 mm of the cornea, now frequently use light-emitting diodes (LEDs) as light sources to produce corneal light reflections. Examples of handheld devices that use LEDs include the Alcon PAK,[10] the Marco-Nidek KM500,[11] and the Retinomax K-Plus.[11]

Corneal Image

The cornea is usually thought of as a refracting element, as it is responsible for most of the optical power of the eye. Since the tear film is reflective, it also acts as a mirror and has reflective properties. Jan Evangelista Purkinje (1787-1869) and Louis Joseph Sansone (1790-1841) studied the properties of these images, which arise from Fresnel reflectivity. The relatively large index of refraction difference between air (index of 1.00) and tear (index of 1.33) causes less than 1% of incident light to be reflected, depending upon the angle.[5]

The cornea can then act as a small (radius of curvature typically around 7 mm) convex mirror. For a given cornea, object size, and object distance, an upright minified image is formed that is located in the eye. If the object size and distance are known, and the image size can be measured, the corneal radius of curvature can be determined by measurement of the observed magnification.

PARAXIAL OPTICS OF CORNEAL IMAGE FORMATION. Figure 1 shows a diagram of corneal image formation. In the example that follows, calculations are done in the manner of teaching of Jack Copeland, where calculations are done on the basis of vergence formulas.[5] The diagram is also meant to introduce the type of system known as a ring keratoscope, in this case where the ring is formed by 12 discrete LEDs, one of which is shown. Consequently, the object and image are described as having a radius. An image of a circular ring object having radius RR that is formed by a spherical mirror is another circular ring having radius IR.

Eqn 1: Vergence Formula: $U + D = V$

Eqn 2: Lensmaker Version: $1/OD + 2/KR = 1/ID$

where U = vergence of light entering optic, D = dioptric power of optical element (mirror or lens), and V = vergence of light exiting optical element, as described below.

U, the vergence of light striking the cornea tear film, is the reciprocal of the distance from the object to the cornea (the object distance OD in Figure 1). Careful inspection of Figure 1 shows that in addition to the distance from the object plane to the corneal apex, there is a small distance arising from the sag of the mirror as it moves away from the optical axis. This sag error (SE) is neglected as a first-order solution to image size, and although the error is negligible in the central 4-mm diameter of the cornea, it becomes significant in the peripheral cornea. For example, for a 7.4-mm corneal radius of curvature, and a sampled corneal area 2 mm in radius, this sag error is 280 µm, and the object distance is tens or hundreds of millimeters. The discussion that follows is therefore

limited to keratometry rather than corneal topography (see below) where aberration corrections are made for accurate measurements of the peripheral cornea.[12]

D, the dioptric power of the cornea, is found from the mirror formula where the spherical power of the mirror is given by the formula D = 2/r, where D is the dioptric power of the mirror (plus for concave surfaces and minus for convex surfaces) and r is the radius of curvature of the mirror in meters, KR in Figure 1.

V, the vergence of light exiting the mirror, is found by the vergence formula Eqn 1. The reciprocal of the vergence V determines the location along the optical axis from the mirror to the location of the image. This reciprocal distance is the image distance (ID in Figure 1), and the difference between this distance and the corneal radius of curvature (KR) determines the image location (IL) inside the mirror.

The size of the image (IR) is found by similar triangles from the central ray, which passes from the tip of the object through the center of the radius of curvature. The ratio of image radius to object radius is the same as the ratio of image distance to object distance.

Eqn 3: Similar Triangles: IR/OR = ID/OD

Eqn 4: Image Size: IR = (ID/OD) * OR

The ratio of object distance (OD) to image distance (ID) gives the same ratio as object size (RR) to image size (IR).

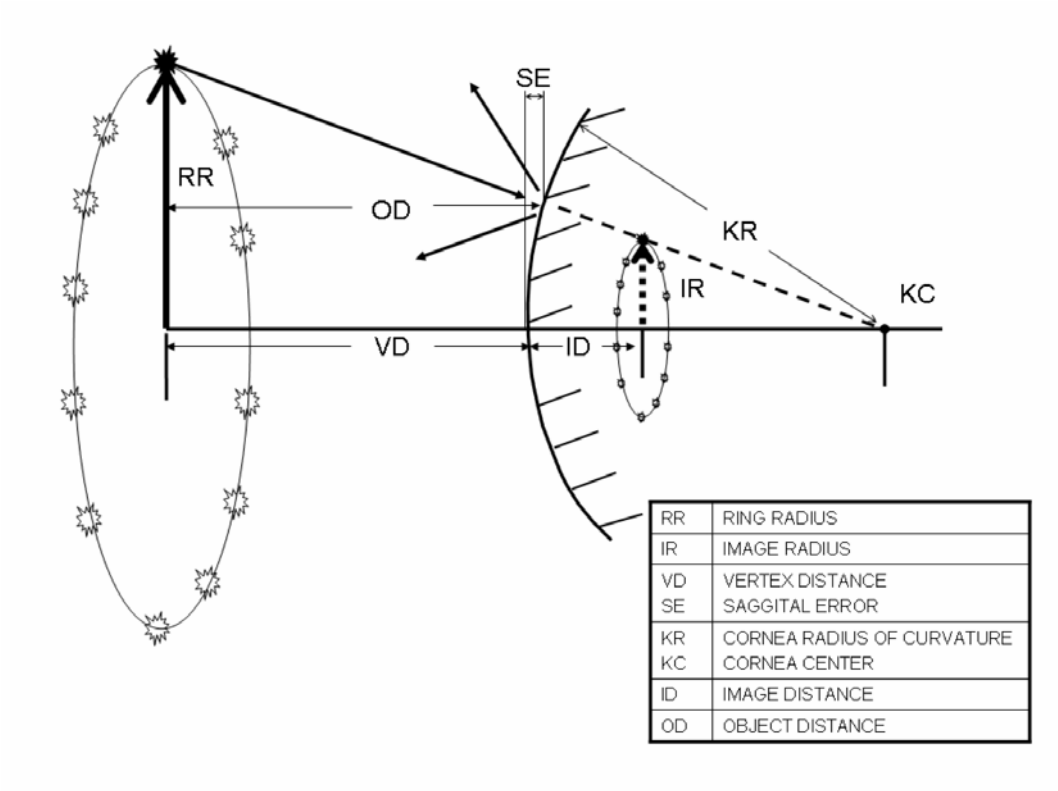

FIGURE 1

Optical ray trace diagram of corneal image formation. A ring of 12 point sources having radius RR is located vertex distance VD from a corneal reflecting surface having radius of curvature KR. A reflected image of the cornea is formed, located at distance ID from the corneal apex, and having image radius IR.

Direct Measurement of Corneal Image Size by an Instrument Operator. In keratometry, the instrument designer specifies the object distance, OD, and provides a means for positioning the patient at the precise distance (usually through a focusing mechanism that has a very shallow depth of focus). The instrument designer can then either control the size of the object (by making the object larger or smaller, until the corneal image size meets a desired end point, as in the Javal-Schiötz ophthalmometer) or measure the size of the image (by use of prisms to measure image separation, as in the American Optical design). In general, instruments in which operators have to align the subject and control the test distance must also deal with the unpredictable eye movements that cause the corneal image to shift as it is examined. For this reason, instruments incorporate image-doubling mechanisms or other methods to cause the reference image to shift with the eye.

Direct Measurement of Corneal Image Size by Image Acquisition and Analysis. Photographic recording of the corneal image allows measurements to be made of an image, where calibrated image magnification allows direct measurement of the corneal image.

The originator of this method was Gullstrand,[13] who defined the general method for measuring the apparent image size photographically in 1893. The work by Gullstrand differentiates a photokeratoscope, where an image is recorded and subsequently measured, from an ophthalmometer, where an instrument operator makes a measurement by visual inspection of a corneal image. When the image is measured photographically, and it is desired to determine the corneal radius of curvature, it is necessary to combine Equations 2 and 3, then solve for the corneal radius of curvature, KR. Equation 5 shows the corneal radius of curvature, KR, as a function of object radius, object distance, and image radius.

Eqn 5: Corneal Curvature: $KR = (2*OD) / ((OR/IR) - 1)$

In equation 5, it is apparent that the determination of the corneal radius of curvature is limited by the accuracy with which the target having object radius, OR (ring of the keratoscope), can be manufactured, by the location of the patient positioned at the object distance, OD (distance of keratoscope ring to subject corneal apex), and by the accuracy with which the size of the resulting image IR (image radius) can be measured.

Measurement of Astigmatism. The astigmatic cornea has two principal meridians, separated by 90°, where the corneal radius of curvature differs. There is a sinusoidally varying change in spherical power between the two principal meridians. With the Placido disc, the reflection of the circular ring is distorted by the astigmatic cornea into an ellipse. With the Javal-Schiötz keratometer, the operator finds the flatter meridian, makes a measurement, and then rotates the target by 90° to find the steeper meridian. For the American Optical style keratometer, doubling prisms allow simultaneous measurement of the corneal power in the two principal meridia.[5] When a reflection of a circular target results in a distorted, noncircular image, the deviations of the image from a circle show the instantaneous, radial power of the cornea at each position on the ring. When an ellipse is fit to the image, the major and minor axis of the ellipse corresponds to the two principal meridia, and the axis of the ellipse corresponds to the axis of astigmatism.[14]

PHOTOKERATOSCOPY AND THE TRANSITION TO COMPUTERIZED TOPOGRAPHY

Keratometry makes measurements of the central cornea to determine the optical properties of the image-forming portion of the cornea. The portion of the cornea overlying the pupil is the active portion in retinal image formation, and typically this area is limited to a 4-mm region. However, as early as Helmholtz, it was observed that the cornea transitioned from a centrally steep portion to a flatter peripheral portion outside the central 4-mm diameter used for image formation. Spherical aberration and large objects located far from the optical axis limit the utility of the paraxial optical equations, and more sophisticated analyses must be employed to determine the curvature and topography of the cornea beyond a 2-mm radius from the corneal apex.

Photokeratoscopy

Historically, the Placido disc[6] was used subjectively for visual inspection of the corneal image. The contribution of Placido was to place a hole with a plus lens that allowed an examiner to inspect the image of the disc. *Photokeratoscopy* is the term for analysis of photographic images from ring keratoscopes, for the photograph can be analyzed, and image sizes determined, if the magnification of the image can be determined.

Mandell extensively studied the peripheral cornea, a portion of the eye that is peripheral to the normal 4-mm pupil and, although not usually involved in image formation, is extremely important for contact lens fitting. He developed the mathematics and instruments to allow calibrated peripheral measurements of the cornea to be made[12] and developed a photokeratoscope that was coupled to a camera and used to photograph the eyes of infants.[15] Using this device, he was able to document the peripheral flattening of the cornea. Further studies of infant refractive error were performed by Howland and Sayles,[16] in which a camera was fitted with a ring of discrete light sources to form a ring keratoscope and isotropic photorefractor.

Photokeratoscopy initially involved the measurement of images of Placido discs that were photographically recorded. The CorneaScope (Kera Corporation) used Polaroid film to record the corneal images of the Placido disc[4] and is perhaps the last photokeratoscope that achieved commercial success prior to the coupling of a personal computer with a video camera. For each ring of the keratoscope, a radial measurement of the ring position was made with respect to the center of the ring. A corneal contour map could be calculated as the apparent radius of curvature changed across the cornea. In 1984, Klyce[17] presented a detailed description of the computerized methods employed to develop three-dimensional reconstructions of the corneal surface contour from digitized photokeratoscope film images. These computations were performed on a timesharing system (PDP-11/34), and the method was not widely available because of the special equipment required for digitization of the photographic film. From this computational basis, a revolution in measurement of the cornea followed with the widespread availability of the personal computer.

Modern Corneal Topographers

Corneal topographers represent the current state of the art in measurement of the surface contour of the human cornea. These devices reconstruct the surface profile of the cornea and are currently the standard of care for diagnosis of keratoconus and other corneal pathology and for planning laser vision correction surgical procedures. The methods employed started with application of ring keratoscopes (Computed Anatomy TMS-1 and EyeSys), then alternate methods of corneal curvature mapping were developed.[18]

As the computational methods of reconstruction of the corneal surface have evolved over time, the limitations of ring keratoscopes have been recognized. Because the rings allow measurement of discrete locations radially (as the transition from the presence to the absence of a bright reflection can be detected), only direct measurement of “radial” power can be calculated. However, the cornea can exhibit changes in contour tangentially that in theory can be missed by a ring keratoscope.[19]Another problem that is inherent in the Placido disc technology is the “black hole” in the center of the cornea, where there is no information due to the absence of a ring.

In order to address these changes, several different technologies have been developed to increase accuracy and overcome the limitations of Placido disc designs. These changes include the development of a checkerboard pattern of targets, where rings alternate from black to white, allowing for both radial and tangential change measurements to be made (AstraScan, LaserSight), a scanning slit system (Orbscan, Orbtek), and pattern projection (PAR systems).[20]

Wavefront Sensors and the Measurement of Higher-Order Aberrations

The use of corneal topography has been complemented in recent years by the development of wavefront analyzers, devices that measure the aberration content of the eye and incorporate information from all four refracting surfaces of the eye (front and back of the cornea, front and back of the lens). These devices, summarized by Schwiegerling,[21] have gone through much of the same evolution of interpretation and analysis as corneal topographers did following the advent of personal computer technology. These devices determine the total aberration content of the eye and, as such, are essential for planning surgical procedures. Just as astigmatism can be either corneal or lenticular in origin (as first described by Thomas Young), making a surgical decision on the cornea without consideration of the lens would be prone to error.

The higher-order aberrations of the eye are errors of the optical system that cannot be corrected with simple spectacles having spherical and astigmatic lenses.[21] These aberrations are modeled by Zernike polynomials, which are a series of surfaces to describe the corneal topography[22] or the wavefront error.[23] The cornea is the principal refracting surface of the eye, and the front surface of the cornea is the predominant refracting element of the cornea.

Higher-order aberrations are frequently measured using a device known as a Shack-Hartmann sensor array, where a rectangular grid of lenslets deflect portions of the wavefront to produce a distorted gridwork of spots. There is an extensive mathematical basis for analysis of such spot patterns, and well-developed methods exist for converting a distorted gridwork of spots into knowledge of the lower- and higher-order aberrations of the eye. While the use of a ring of discrete LEDs is useful for fitting an ellipse to the image for subsequent determination of corneal spherical power and astigmatic power, a rectangular gridwork offers advantages for the determination of higher-order aberrations.[21]

After spherical defocus and astigmatism, the higher-order aberrations result in impaired image formation on the retina and presumably can result in decreased visual acuity and amblyopia. Of the higher-order aberrations, spherical aberration and coma are the most frequently encountered and are now the topic of study on their effects on visual development.

Thus, in measuring the corneal surface for its effects on image formation in the eye, the most important aberrations are the lower-order aberrations of sphere and cylinder. Investigation of spherical aberration and coma affecting image formation, for the area of the cornea lying over the pupil, is of research interest.[24,25]

GOALS OF THE PRESENT PROJECT

The purpose of the present project is to build upon prior work on the development of keratometers for the measurement of the infant and toddler eye for the presence of corneal astigmatism, and to provide a research platform for the measurement of higher-order aberrations that are visually significant and occur over the naturally occurring pupil.

In developing such an instrument, several design factors were identified and are discussed below.

Testability

First and foremost, the design should provide a clinically useful measurement method that could be used in a high proportion of infants and children. The instrument must be both infant and toddler friendly, highly usable by the operator, and likely to perform similarly regardless of the training of the individual operating the instrument. In other words, it must be acceptable to the infant and toddler and usable by the staff.

Sufficient Accuracy for Characterization of Corneal Astigmatism

The goal of the present research is not to develop a new corneal topographer or wavefront analyzer that would advance the state of the art in either measurement accuracy or measurement range, but rather to develop an instrument specifically for the longitudinal measurement of astigmatism in infants and toddlers who are too young to use conventional instrumentation. A highly accurate instrument that is designed to be used by an adult who is seated with the chin placed in a chin rest and gazing purposefully at a fixation target for as long as it takes the operator to align the instrument and obtain an image will not work for infants and toddlers. Degraded accuracy is acceptable if the tradeoff is high testability. Rather, the goal is to develop a handheld instrument that will be tolerated by an infant or toddler as the examiner entertains the child in other ways, such as making eye contact, showing a finger puppet, or talking to the child while making eye contact.

Potential for Measurement of Higher-Order Aberrations

Ring keratoscopes can be used for the determination of higher-order aberrations of the cornea, subject to the limitations imposed by the fact that the ring provides radial but not tangential changes in the image. This limitation is overcome by the use of discrete light sources or targets that have transitions in both the radial and tangential paths around the cornea.

A rectangular grid in image space is an appealing image to analyze, as there are readily available algorithms for analysis of such images. Spherical error is indicated by relative magnification or minification of the square grid. Vertical or horizontal stretching of the grid into rectangles indicates the presence of with-the-rule or against-the-rule astigmatism. Stretching of the square pattern into a regular array of parallelograms would indicate oblique astigmatism, whereas distortions that vary across the grid would demonstrate the presence of higher-order aberrations. Squares that enlarge or contract radially would indicate the presence of spherical aberration,

and squares that are narrower on one side than the other would indicate the presence of coma.

There are numerous examples of such distorted grid arrays in the literature for interpretation of Shack-Hartmann sensor wavefront data, and our group has developed a handheld, open-field Shack-Hartmann sensor for use with infants and toddlers (Schwiegerling J, ARVO Annual Meeting, 2005, Abstract). A goal of the present instrument development project is to create such a rectangular grid in the corneal image as a topic for future investigations and algorithm development, in order to correlate corneal aberration content in our subjects with wavefront error that is measured with the handheld, open-field pediatric wavefront evaluator (PeWE).

Building Upon Prior Hardware and Software Development

Our research team had built four prior keratometers for the investigation of infant astigmatism. Each has built upon the other, and each has advanced the art to some extent. The topic of this thesis is infant keratometer number 5, or IK5. Briefly, infant keratometers 1 through 4 will be reviewed below in order to see the development of the current design, described in the "Methods" section to follow.

IK1, known as the video remote keratometer,[14] was a large instrument (Figure 2) that operated at a distance of 1 meter from the subject. It was a two-ring keratoscope that alternated illumination of the rings and performed digital subtraction of the images in order to isolate the discrete reflections from the infrared LEDs. Both eyes were imaged at the same time, and subpixel image processing methods were used to determine the corneal power from a relatively small image of the eye, a result of imaging both eyes within the same frame. A singular value decomposition (SVD) chi-square minimization routine was used to fit the five parameters of the ellipse to the ring data.[26] The corneal curvature that was determined was then incorporated into an optical model to interpret the images for the presence of strabismus.[27,28]

IK2, developed for an unfunded grant application, was a handheld keratometer and phakometer that implemented the technique of Howland and Sayles[16] with video recording of infrared images. This instrument was constructed using a solid state (CCD) infrared camera and utilized the Sony HD format for individual addressing of stored frames. Just as noted by Mandell,[12] who had to flash photograph the infant more than a dozen times to obtain a single usable image, video recording of many images was necessary for subsequent selection of the best images for processing.

IK3, the first version to incorporate a handheld keratoscope on camcorder, is shown in Figure 3. As the camcorder was not sensitive in the IR, visible LEDs were used. The device incorporated a plexiglass disc that could be used to view the child under study. The operating distance was 180 mm, a distance that was determined by measuring the length of several baby bottles. The device recorded data onto the Sony High-8 format video tape, and computer controls were developed to allow individual frame access. Four computers were required to control the tape drives, capture the images, and then process them.

FIGURE 2

IK1, the video remote keratometer, used to obtain simultaneous binocular measurements of corneal astigmatism and ocular alignment from a distance of 1 meter. This device included two rings and incorporated a coaxial infrared light source that permitted measurement of strabismic deviations through the measurement of both eyes' Purkinje reflexes.

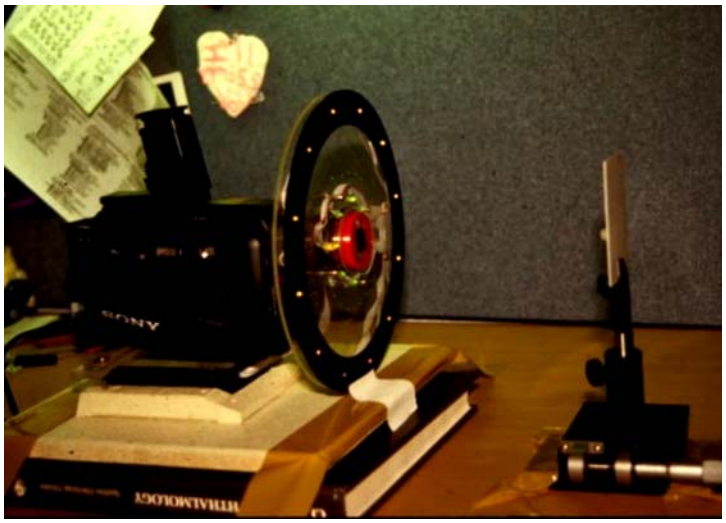

FIGURE 3

IK3, the handheld infant keratometer, utilizing a clear plexiglass disc of 200-mm diameter, and 12 visible light-emitting diodes in the outer ring. This device used analog video recording methods. The clear plexiglass disc allowed the examiner to establish eye contact with the subject.

IK4, the digital infant keratometer shown in Figure 4, was developed following the marketing of consumer digital recording camcorders with high infrared sensitivity. The camera was a digital device that greatly increased the image quality and permitted greatly simplified playback and image selection. The keratoscope was a single 200-mm ring device that also had a 180-mm working

distance. Experience with IK3 found that the child frequently looked around the center of the ring to see the operator, resulting in frequent off-axis measurements. For this reason, IK4 had a completely obstructed ring, and the operator would look at the child, then hide behind the disc, allowing the child to look at a central visible LED that was seen through a small beam splitter (rectangular device in the center of the disc behind a glass filter).

A special telecentric lens was developed for IK4 that allowed images to be obtained of the cornea where the magnification remained relatively independent of position (Miller JM, ARVO Annual Meeting, 2005, Abstract). The telecentric lens allows a field of view of 25 mm at a distance of 180 mm but provides little to no magnification change over its depth of field of 3 cm. Having the image size remain constant regardless of vertex distance overcomes a confounding factor in the measurement of astigmatism, namely, inaccurate measurement of image size. As the image went in and out of focus, the distance between corneal light reflections remained unchanged.

Special software was developed by Jim Schwiegerling for automated selection of good images from a tape segment, eliminating a very tedious manual task. This software automatically scans the tape for the presence of a ring of 12 bright spots (from 12 IR-LEDs) and then selects and isolates the frames having the sharpest focus and best centration with regard to the pupil. An ellipse is then fit to the ring of LEDs and astigmatism is measured. The system then averages multiple frames to provide a best estimate of corneal astigmatism.

IK4 has been in use for over 3 years (Donaldson CC, ARVO Annual Meeting, 2007, Abstract) in a study of infant visual development directed by another member of our group, Erin Harvey, PhD. The role of corneal astigmatism and higher-order aberrations in the eyes of Native American infants and toddlers is being evaluated in this National Institutes of Health–funded study (NEI-NIH 13153).

Open-Field Design

IK5, the designation given to the open-field infant keratometer described in the "Methods" and "Results" sections of this thesis, has a markedly different form factor than instruments IK1 through IK4 (Figure 5). While it is handheld, it is also open-field to allow unobstructed eye contact between the examiner and the infant or toddler. Our experience with the IK3 was that the children tended to look to the clear area of the disc at the examiner, resulting in an off-axis image. We found with IK4 that babies and toddlers found the single central visible LED to be too boring to pay attention to, and it required considerable effort to get them to look at the camera. Our first experience with an open-field instrument is the PeWE, and it has proven to be very usable with children.

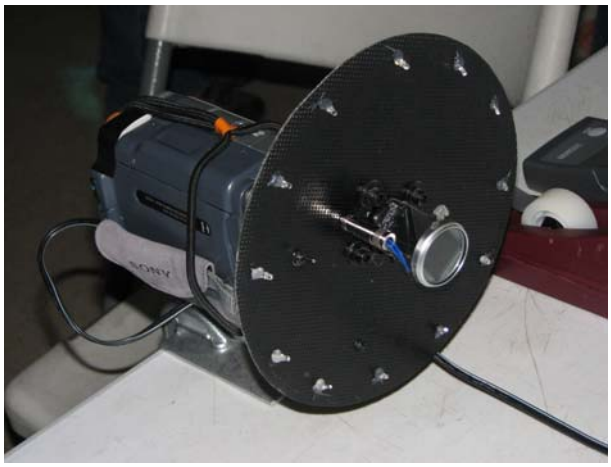

FIGURE 4

IK4, the digital infant keratometer, now used to measure corneal astigmatism in a study of the effects of astigmatism on infant visual development. The device utilizes a digital recording system, making the individual isolation and analysis of video images much more practical, with higher resolution than obtained with analog recordings. The infrared light-emitting diodes are on a radius of 90 mm; a telecentric lens allows measurement of corneal images at a distance of 150 to 175 mm without associated magnification changes. A beam splitter is on-axis and provides a single dim green fixation target for the child to view.

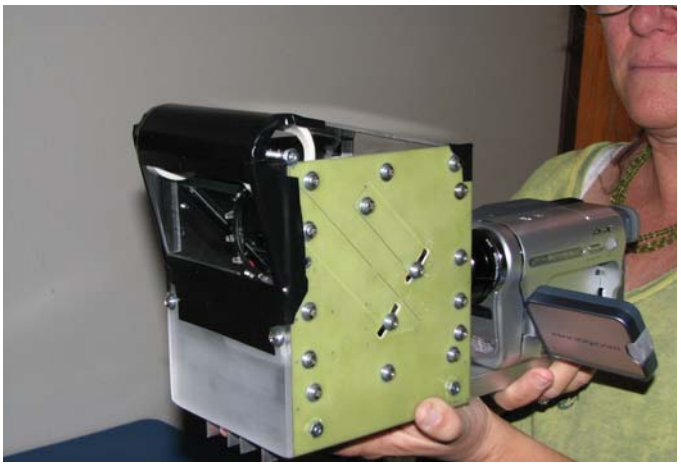

FIGURE 5

IK5, front view of the open-field infant keratometer. The keratoscope ring of infrared light-emitting diodes (LEDs) is visible. The ring of LEDs are centered about the subject's right eye. Mirrors that reflect infrared light but pass visible light allow the operator to make eye contact with the subject. The working distance of this device from the subject is between 15 and 40 mm from the faceplate of the keratometer. The optical head is fully enclosed, allowing for easy cleaning and decreasing the risk of dust accumulation.

For a beam splitter and grid array to be incorporated into the open-field design (in order to study the higher-order aberrations within the corneal apex), the working distance is small (25 mm). It includes a ring keratoscope that samples a similar area of the

cornea as IK4, in keeping with the concept of the device being a keratometer rather than a corneal topographer.

Robust Construction

The IK4 is constructed of perforated circuit board prototyping material and has exposed wires that are attractive to little fingers. The IK5 construction method should be more robust in that all wiring is fully enclosed, without any sharp edges or potential hazards.

METHODS

The handheld open-field infant keratometer (OFIK, IK5) provides unobstructed eye contact with an infant or child in an instrument that is an optical head mounted to a digital camcorder. The camcorder and telecentric imaging system have been previously described (Miller JM, ARVO Annual Meeting, 2005, Abstract). The present design incorporates the camera and telecentric lens that is used in IK4, but replaces the ring keratoscope with an optical head that includes two beam splitters and a mirror.

LIGHT PATH FROM SUBJECT TO CAMERA

In the instrument plan (Figure 6) there are three mirrors. Following the path from the subject's eye to the camera, mirror M3 is a partially reflective warm mirror. The front surface of mirror M3 is specified to reflect 10% of infrared light, whereas the uncoated rear surface reflects about 2% of infrared light. Most (about 88%) of the light from the eye is transmitted through mirror M3 and then strikes the first surface of mirror M2, which fully reflects IR and fully transmits visible light. Thus, the observer and the subject can see each other in visible light, but the IR light from the subject's eye is reflected downward to mirror M1, which is a fold mirror that turns the light into the camera lens. The total design distance from the subject's eye to the camera lens is approximately 180 mm, as in the IK4.

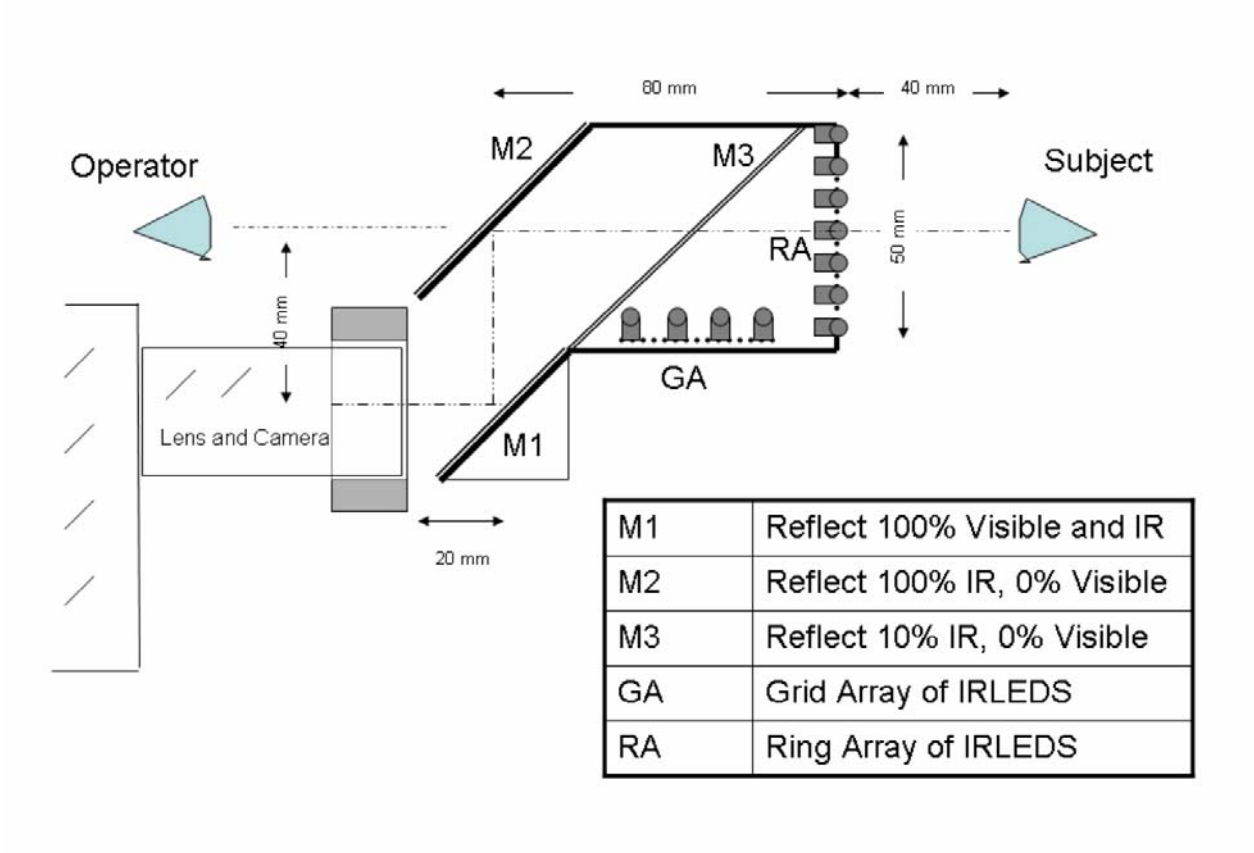

M1	Reflect 100% Visible and IR
M2	Reflect 100% IR, 0% Visible
M3	Reflect 10% IR, 0% Visible
GA	Grid Array of IRLEDS
RA	Ring Array of IRLEDS

FIGURE 6

IK5, side view diagram of the open-field infant keratometer. Three mirrors provide illumination that is coaxial with the imaging system, allowing for creation of a grid array of spots within the ring image. The ring of infrared light-emitting diodes (IRLEDs) that are used for conventional keratometry has a diameter of 50 mm and is a nominal distance of 40 mm from the subject. The grid array of IRLEDs allows for measurement of the corneal apex, an area that is normally not measured in conventional keratometery because of the "black hole" in the center of the keratoscope caused by the camera lens.

The instrument is fully enclosed. Window glass is used for the faceplate window closest to the subject, and acrylic resin is used for

the other windows. The tilt to the roof and front window is necessary to avoid reflections.

The instrument is constructed using computer-aided design construction. The critical machining of guide holes for mounting the three mirrors was performed by using printed circuit board design tools. Both mirrors have tip adjustment to permit alignment of the optical system.

LIGHT PATH FROM INFRARED LEDS TO SUBJECT

Infrared (880-nm) LEDs (IRLEDs) were used to illuminate the cornea and create a corneal image. The ring of 12 small (T3) IRLEDs is mounted on a small circuit board that is mounted vertically behind the front window of the device. There is approximately 15 mm of optical distance from the light source of the IRLEDs to the outside surface of the faceplate window, not equal to the linear distance because the IRLED incorporates an optical element in its construction. The eye relief, from the subject's eye to the faceplate, is approximately 25 mm or 1 inch. While the ring array (RA) is readily visible when the device is held away from the subject, once the device is brought close to the eye, the ring is not readily apparent and does not obstruct the view straight through to the operator's face and eyes.

Located perpendicular to the ring array is the grid array (GA), which is constructed of 12 larger (T1) IRLEDs that project their light upward. Most of the light passes through the mirror, but some (10% from the front surface and approximately 2% from the rear surface) is reflected toward the subject and illuminates the cornea, creating a corneal image.

Figure 7 shows the pattern of illumination that is seen in the infrared (but not seen by the subject). Note that because of the selection of a thick mirror for mirror M3, the 12 IRLEDs are effectively doubled into 24 discrete point sources. This image was obtained using a second IR video camera during the mirror alignment process. The IRLED arrays are powered by a 9-V battery, and each array is independently voltage regulated to ensure constant light levels as battery voltage declines to 7 V.

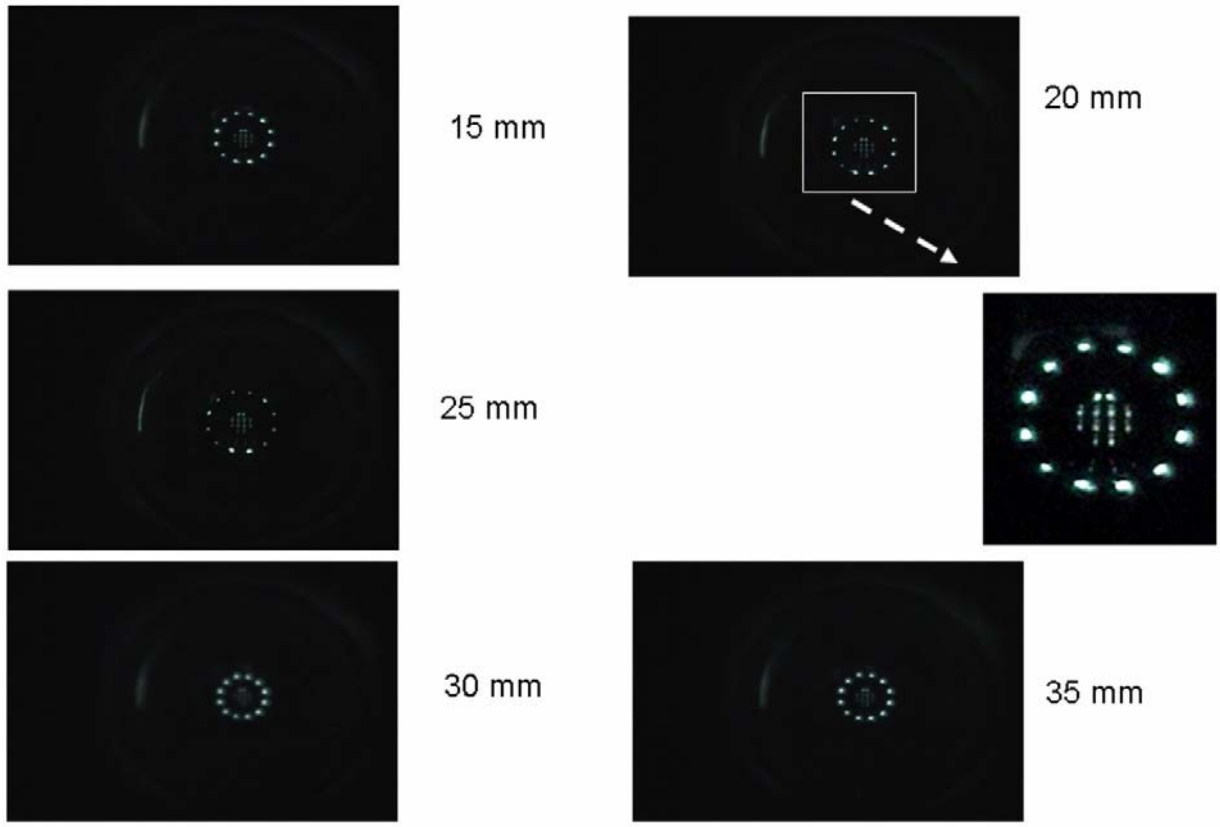

FIGURE 7

IK5, the open-field infant keratometer, infrared (IR) images. In each image (obtained at the vertex distance of reflecting ball to the faceplate of the instrument), the outer circular ring arises from the ring array, whereas the central grid pattern arises from the superposition of the grid array made possible by the use of IR beam splitters. A detail of the grid array image is shown center right.

IMAGING SYSTEM

A telecentric lens was developed for IK4 and used in conjunction with the Sony TRV-460 camcorder (Miller JM, ARVO Annual Meeting, 2005, Abstract). The camcorder required a simple modification to allow exposure control while recording in the infrared. The camcorder was set for infinity focus, and the zoom was set for a field of view corresponding to 25 mm at a distance of 180 mm. The telecentric lens design then brought the focus forward to 180 mm. A characteristic of a telecentric lens is that only rays of light that enter parallel to the optical axis are imaged, and the remaining rays are excluded by the stop. Because only parallel rays are imaged, over the range of focus magnification changes should not be observed in the image. An effective telecentric lens imaging a ring of discrete IRLEDs should have a small, tightly focused image at optimum focus, and although the image of each point source may enlarge and become a larger blob either side of focus, the size of the ring should be unchanged.

To verify that the camera zoom and focus settings, in conjunction with the telecentric lens, were achieving this goal, a telecentric calibration target was constructed and is shown in Figure 8. A circuit board was fabricated with a central 0.250-inch hole surrounded by 12 0.029-inch holes on a 5-mm radius. Mounting holes in the corner of each circuit board allowed the boards to be precisely stacked and the central hole and each of the 12 smaller radial holes to be aligned. The rear board was covered on its rear surface with a diffuser and illuminated with an IRLED (not shown, but mounted on the third circuit board). The spacing between the first and second board was 0.75 inches, and the central hole was filled with a 0.25-inch OD hollow cylinder. If the lens is set in a telecentric manner, then the bottom of the central hole should be seen full size (not smaller), and each of the 12 holes should be lighted.

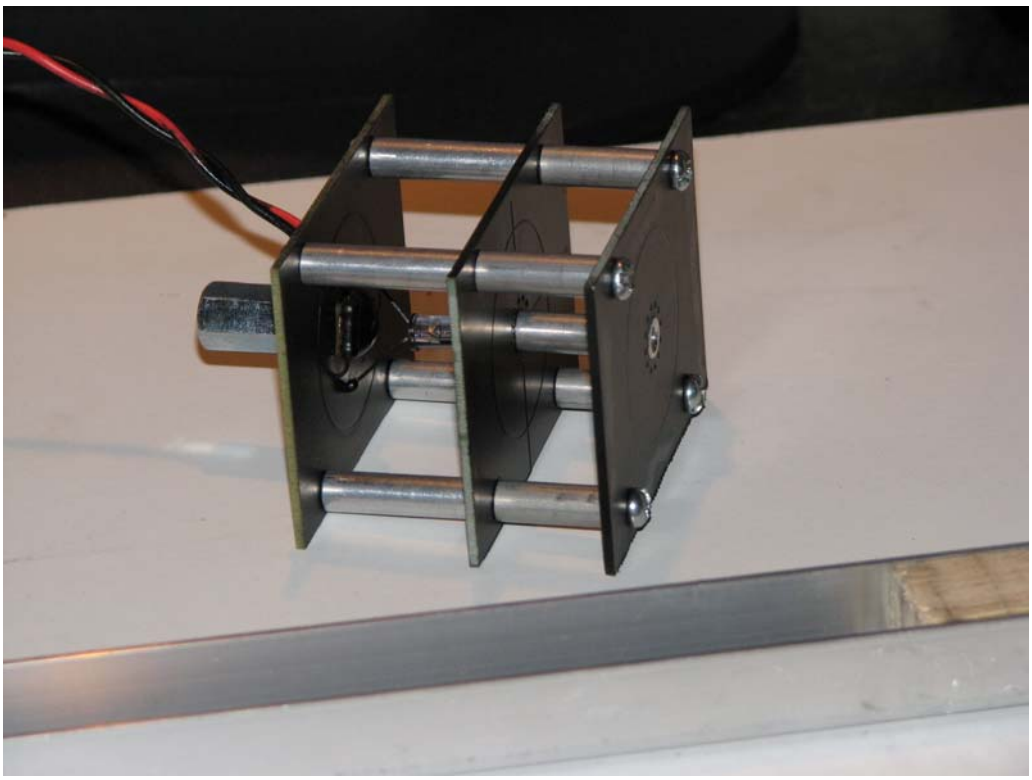

FIGURE 8

Telecentric target. The telecentric calibration target is constructed from robotically manufactured circuit boards that allow high dimensional accuracy at relatively low cost. The hole pattern creates a ring of 12 holes spaced at 5-mm radius. The sandwich stack of circuit boards overlying each other limit illumination through the frontmost set of holes to light rays parallel to the optical axis. This novel telecentric target allows for calibration of the imaging lens (because of known spacing of the holes on a 1-cm diameter) and verification that the lens is in its telecentric setting (by observing illumination through the sandwich of circuit boards).

STEEL BALL CALIBRATION

Six steel balls with diameters of 0.375, 0.500, 0.563, 0.594, 0.625, and 0.750 inches were used for calibration of the open-field infant keratometer. In order to mount the balls and precisely position them where a subject's cornea would be located, a calibration fixture was constructed that allowed 5 degrees of freedom. A circular magnet was mounted on the end of a 20-turn-per-inch lead screw and was used to hold the steel balls when they were being imaged. There was sufficient travel to allow the balls to be moved across a sufficient range of focus to determine the distance from the faceplate where optimum focus was achieved. This test fixture also served

to position the telecentric focus aid. Using this apparatus, it is possible to precisely position the steel balls across a range of distances from the faceplate and to change the vertex distance from ball to faceplate without the steel ball translating horizontally or vertically within the image.

The steel ball calibration was essential for two purposes. First, it allowed the determination of the effective position of the IRLED point sources within the optical casing and the accurate determination of the object distance from IRLED to steel ball vertex. Second, by establishing calibration, it was then possible to determine in a group of human subjects who had known keratometry values the actual vertex distance at which the handheld image was recorded.

HUMAN SUBJECTS EXPERIMENTS

Two groups of subjects were then imaged with the device.

Adult Subjects

First, a group of 16 adult volunteers had keratometry performed with a Retinomax K-Plus (Right Mfg Co, Ltd, Tokyo, Japan). Each subject then had approximately 30 seconds of video recorded using the open-field infant keratometer. This experiment served two purposes: (1) to verify that there was sufficient illumination from the IRLEDs to reliably create corneal images that could be recorded, and (2) to determine how narrow the apparent range of best focus was in the recorded images through back calculation of vertex distance from known corneal curvature.

Infants and Toddlers

Second, a group of 10 infants and toddlers had keratometry performed in order to determine how acceptable the instrument was to both the subjects and the investigator, and to determine if usable images could be obtained. This human factors study did not result in quantitative measurements of corneal curvature, but was performed to verify that the instrument produced interpretable images and that the operator found the device usable in making measurements on infants and toddlers.

SUBJECTIVE INTERPRETATION OF GRID ARRAY IMAGES

A final analysis was performed on the images from the human subjects to determine subjectively if the grid array imaged within the ring was sufficiently bright and distinct to warrant further investigation as a means of measuring higher-order aberrations within the confines of the central cornea. This experiment was for proof of concept of the open-field design in being able to both illuminate and image within the ring keratoscope.

IMAGE PROCESSING AND DATA REDUCTION

Images were recorded using the Sony TRV-460 camcorder in NightShot (IR sensitive) mode. Recordings were then played back and transmitted by FireWire interface to a computer running Microsoft Windows Movie Maker, and transferred to AVI format for subsequent analysis. The shareware program Advanced AVI Splitter (http://www.aviexpert.com) was used to review the recorded video frame-by-frame and to extract the frames of interest as individual bitmap files for image analysis. Each file was examined for frames that appeared sharply focused and free of motion artifact. A single frame was analyzed for each experimental condition. No averaging was used.

Extracted frames were then analyzed using a custom Visual C++ 6.0 program, “centroider,” developed for this project, which measured grayscale centroids with variable-sized kernels ranging from 7 to 64 pixels. This program allowed an operator to position the cursor in the subjective center of the blob representing a corneal light reflection from an IRLED, but by performing grayscale centroiding in a kernel larger than the blob, removing the subjective factor from blob determination. For each image, the subpixel resolution centroid for each of the 12-ring array IRLEDs was determined and stored as a text file. The output of “centroider” was then read by an ellipse-fitting routine, “elfit,” that used chi-square minimization to fit the five parameters of an ellipse to the ring of 12 IRLED image locations. The major and minor axes and orientation of the fit ellipse were then stored as another text file and transferred into Microsoft Excel for final data reduction.

Microsoft Excel was then used for final analysis, data reduction, and graphing. The linear regression functions within Excel were used for curve fitting. Descriptive statistics were generated within Excel. Pearson’s correlation coefficient was calculated for linear regressions that were performed.

RESULTS

TELECENTRIC LENS CALIBRATION

The telecentric calibration target was positioned in the calibration fixture and moved fully forward so the top of the target was touching the faceplate of the instrument, then backed off 20 mm. Images were collected at vertex distances ranging from 20 mm to 55 mm in 5-mm steps. Figure 9 shows the images that were collected at the eight test distances. Careful inspection of the images shows that they are somewhat elliptical, and horizontally elongated. The Sony CCD has a resolution of 720 horizontal and 480 vertical pixels, with an aspect ratio of 4 to 3. Square pixels, as displayed on a video monitor, would have 640 horizontal pixels and 480 vertical pixels for the same aspect ratio. Theoretically, this implied that the vertical pixels should be stretched by 12.5% (720/640) for proper magnification measurements.

By visual inspection of Figure 9, it is clear that the optimal (sharpest) focus was achieved between 20 and 25 mm vertex distance

of target to faceplate. This best focus is seen by the smallest observed spot size for the 12 rear illuminated holes. While this could be quantitated by measuring blob size, it was not felt necessary to do so because the effect was so pronounced.

However, it is not clear by visual inspection whether or not image magnification is occurring with change in vertex distance, if the pixels differ in height and width by 12.5%, or what is the actual calibration of the image in terms of pixels per millimeter image size vertically and horizontally.

The images shown in Figure 9 were analyzed and ellipses fit to each to determine the horizontal and vertical dimensions in pixels. These results, shown in Table 1, demonstrate that over the range of 20 to 55 mm vertex distance, the coefficient of variation was 0.8% horizontally and 1.2% vertically, indicating that the telecentric lens was properly configured.

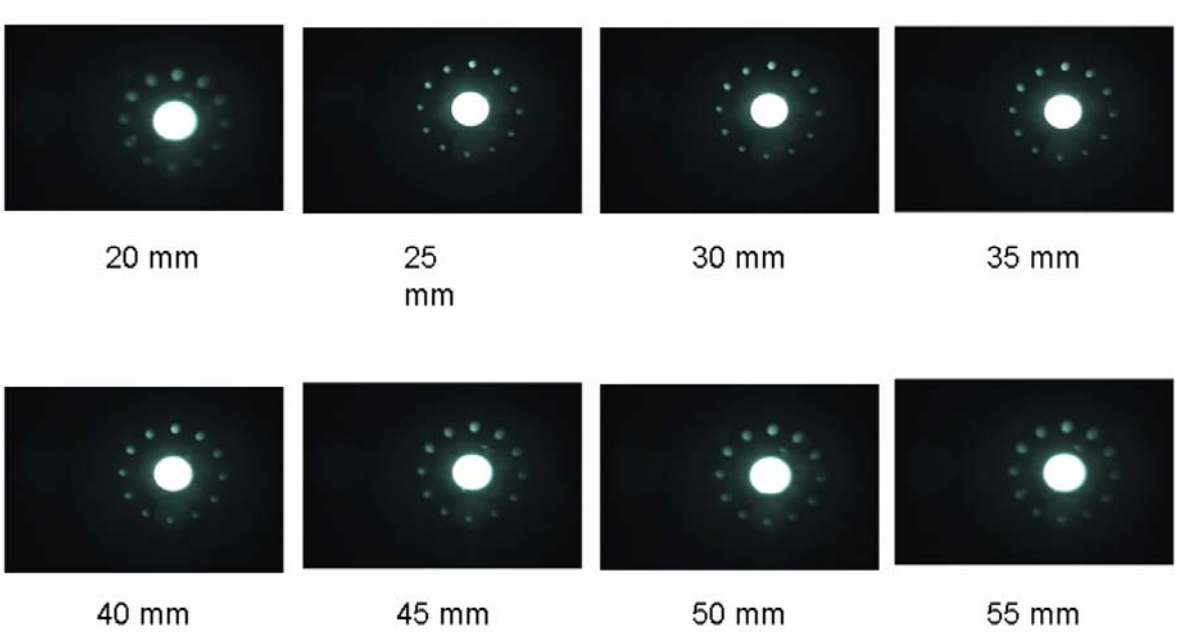

FIGURE 9

Images obtained with the telecentric calibration target, used both to demonstrate telecentric focusing as being present and to determine imaging system magnification by measurement of the 1-cm-diameter ring of illumination. Effective depth of focus is confirmed by the relatively uniform illumination of all holes.

TABLE 1. OBSERVED CALIBRATION IMAGE HEIGHT AND WIDTH, IN PIXELS, FOR 10-MM-DIAMETER CIRCULAR RING, OVER MAXIMUM RANGE OF VERTEX DISTANCES OBSERVED

VERTEX DISTANCE, mm	HORIZONTAL RING WIDTH, PIXELS	VERTICAL RING HEIGHT, PIXELS	HORIZONTAL PIXELS PER mm	VERTICAL PIXELS PER mm
20	125.80	113.78	25.16	22.76
25	125.65	113.61	25.13	22.72
30	126.92	112.82	25.38	22.56
35	126.38	114.74	25.28	22.95
40	127.67	115.26	25.53	23.05
45	127.21	116.03	25.44	23.21
50	127.20	115.45	25.44	23.09
55	128.81	117.08	25.76	23.42
		Mean, pixels per mm	25.39	22.97
		SD, pixels per mm	0.21	0.28
		Coefficient of variation (SD/mean)	0.81%	1.22%

SD, standard deviation.

Steel balls were subsequently imaged, and it was found that useful images could not be obtained at a vertex distance greater than 35 mm. Beyond this vertex distance, images were so defocused that centroids were not reliably estimated, and the images were so clearly out of focus that they would not be subjected to image analysis. If the data are restricted to vertex distances of 35 mm or less,

the coefficient of variation drops to 0.46% horizontally and 0.69% vertically, and the aspect ratio of height to width was found to be 11%, confirming the expected aspect ratio of 12.5%. For the observations obtained at 35-mm vertex distance or less, the theoretical aspect ratio of 12.5% was applied to normalize the horizontal to vertical measurements, and the results were reanalyzed to determine the optimal calibration for height and width. Using this method in which analysis was restricted to the vertex distances where corneal light reflections might be expected to be observed, the calibration factors of 25.41 pixels per mm horizontally and 22.57 pixels per mm vertically were obtained.

STEEL BALL CALIBRATION

The six steel balls were then imaged at vertex distances from 15 mm to 35 mm, and then analyzed to determine the ring image radius in millimeters. While the telecentric lens allows accurate measurement of image size across a range of vertex distances, it does not prevent the actual image size from changing with vertex distance. The greater the vertex distance, the smaller the proportional change in image size from an incremental change in vertex distance, as follows from Equation 3. For each of the six steel balls, the observed change in image size is shown in Table 2 and graphically displayed in Figure 10. In this series of observations, the true vertex distance was known by measured placement of the steel balls away from the faceplate of the instrument. There is considerable variation in observed image size over a 5-mm shift in actual vertex position.

TABLE 2. IMAGE SIZE VARIATION WITH VERTEX DISTANCE

STEEL BALL	VERTEX DISTANCE mm, BALL TO FACEPLATE	IMAGE RADIUS, mm
Ball 1:	15	1.60
4.76 mm radius,	20	1.43
70.87 D refracting Power	25	1.34
	30	1.23
	35	1.15
Ball 2:	15	2.07
6.35 mm radius,	20	1.89
53.15 D refracting power	25	1.70
	30	1.55
	35	1.42
Ball 3:	15	2.36
7.15 mm radius,	20	2.12
47.2 D refracting power	25	1.93
	30	1.74
	35	1.61
Ball 4:	15	2.46
7.54 mm radius,	20	2.21
44.74 D refracting power	25	2.01
	30	1.83
	35	1.68
Ball 5:	15	2.61
7.94 mm radius	20	2.36
42.52 D refracting power	25	2.14
	30	1.96
	35	1.79
Ball 6:	15	3.06
9.53 mm radius,	20	2.77
35.43 D refracting power	25	2.52
	30	2.30
	35	2.10

The data in Table 2 were obtained over a very large range of vertex distances, and some of the images appeared subjectively to be much better in focus than others. Figure 7 shows the images from ball 4, having 7.54-mm radius, across the range of vertex distances. While the images obtained at 15, 20, and 25 mm are seen to have relatively sharp focus, the images obtained at 30 mm and 35 mm vertex distance were notably blurred and subjectively would not be selected for analysis. By inspection, it appears that the range of focus for the handheld instrument might be expected to be about 10 mm, from a vertex distance of 20 mm to 30 mm, with best focus around 25 mm, or 1 inch. This is in keeping with the instrument design and the telecentric target test.

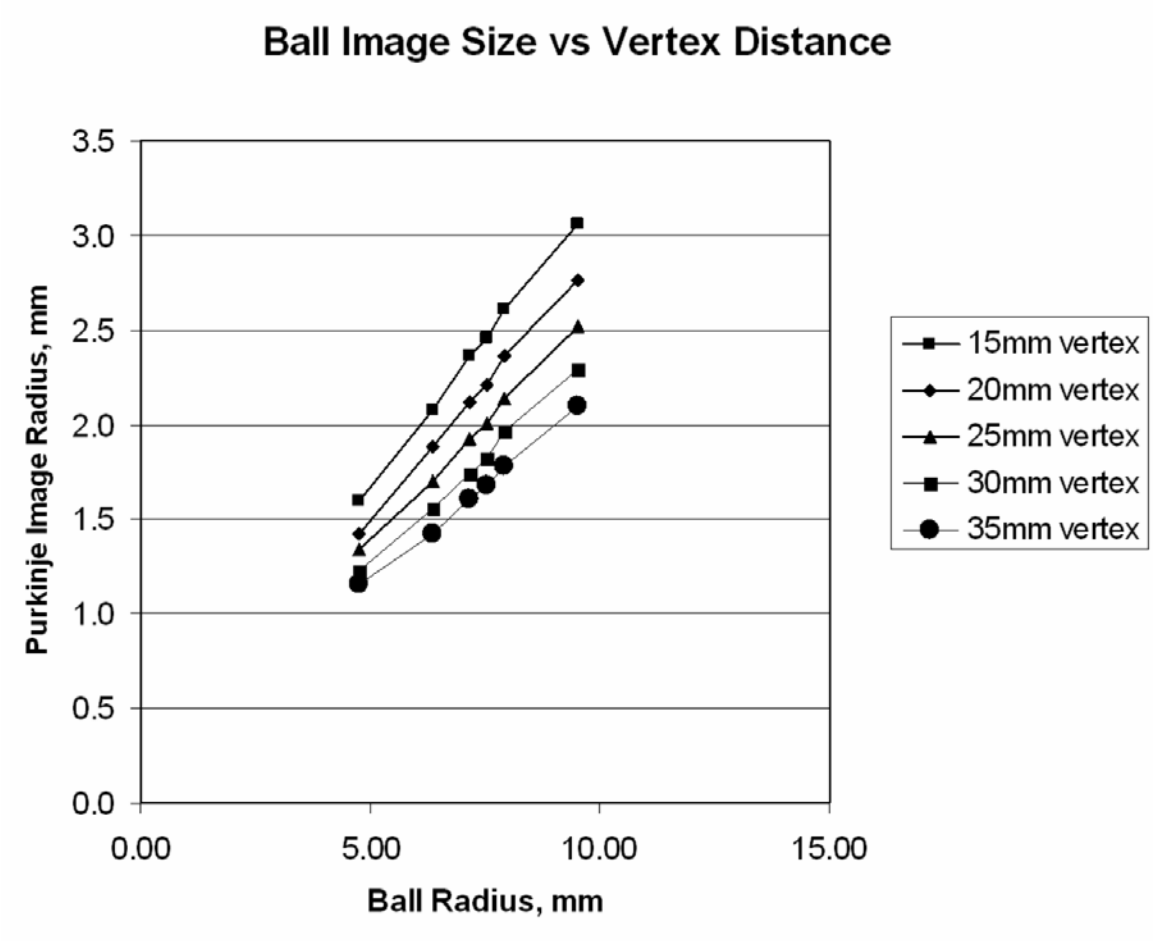

FIGURE 10

Vertex distance effect. Graph of image size vs vertex distance for the corneal image of the ring array. Six steel balls were measured at 5 different vertex distances, and the image radius was determined for each of the vertex distances. The data were obtained from measurements made using the open-field keratometer at vertex distances ranging from 15 to 35 mm.

HUMAN SUBJECTS

Adult Subjects

The results for the 16 adult subjects are shown in Table 3. For these subjects, keratometry was measured independently with the Retinomax K-Plus, allowing for determination of the actual vertex distance at which the image was obtained. This determination was made by back calculation from measured corneal radius (from the Retinomax measurement), actual object size, and observed image size. In this manner, the actual vertex distance at which the image was recorded was determined for each of the 16 adult subjects when the instrument was used in handheld mode by the operator, and the subject was free to move. Approximately 30 seconds of recording was taken for each of the subjects, and the subjectively determined sharpest image for each subject was selected.

In this manner, a range of actual vertex distances was determined for the subjects, from 18 to 27 mm, with average value of 22 mm. Given that 22 was the average for the group, it is taken as the expected value of vertex distance for all subjects. With this expected value of vertex distance determined for the group, the corneal curvatures were recomputed as would be expected for a subject where keratometry was not known a priori. These calculations result in the final two columns of Table 3, where the instrument error is determined by comparing observed corneal curvatures measured with the Retinomax K-Plus with those measured with the open-field infant keratometer, at an expected vertex distance of 22 mm.

Depending upon the needs of the researcher, this instrument may or may not provide acceptable performance. If the researcher desires to characterize the magnitude and amount of astigmatism present in an infant subject, the accuracy may be sufficient. In the measurement of astigmatism, the mean difference in repeated measurements was 0.27 D, with a standard deviation of 0.45 D. This accuracy is sufficient to characterize a subject as having no or low astigmatism, moderate astigmatism, or high astigmatism. However, astigmatism is determined by the difference in corneal power along the major and minor meridia. If the powers of the two principal

merida are either underestimated or overestimated, but move in the same direction, the measurement of astigmatism may be more accurate than that of the underlying meridional powers. Such is the case with this instrument. With changes in vertex distance, the absolute power of the cornea meridia, or the absolute radii of curvature of the cornea, is not sufficient to allow accurate descriptions of the shape of the cornea and longitudinal studies of change. The standard deviation of repeated measurements of meridional power is 3 D, six times greater than that of repeated measurements of astigmatism (0.45 D). The instrument may be accurate enough for studies of astigmatism but not for studies of absolute corneal curvature.

TABLE 3. ACCURACY OF OPEN-FIELD KERATOMETER WHEN USED WITH COOPERATIVE ADULT SUBJECTS IN HANDHELD MODE

SUBJECT	BACK CALCULATED VERTEX DISTANCE, mm	VERTEX DISTANCE ERROR FROM 22-mm GROUP MEAN	ACTUAL CYL, D, DETERMINED BY RETINOMAX K-PLUS	SEQ ERROR, D, CALCULATED ASSUMING VERTEX DISTANCE OF 22 mm	CYL ERROR, D, CALCULATED ASSUMING VERTEX DISTANCE OF 22 mm
1	21	-1.0	0.63	-1.24	-0.22
2	24	1.9	0.79	1.11	0.96
3	20	-2.1	1.14	-2.72	0.02
4	20	-2.2	0.83	-2.69	0.11
5	26	4.5	0.93	3.72	0.58
6	20	-2.4	1.39	-3.11	-0.09
7	23	1.2	0.76	0.87	-0.01
8	22	0.0	0.73	-0.59	0.41
9	26	3.8	0.23	3.37	0.80
10	26	3.7	0.35	3.25	0.68
11	20	-1.9	3.24	-3.26	-0.67
12	25	3.4	0.96	3.00	0.03
13	18	-4.3	2.69	-6.35	0.93
14	20	-1.9	0.32	-2.24	0.23
15	21	-0.7	0.42	-1.13	0.34
16	18	-4.4	0.77	-4.96	0.47
Mean	22.13	0.13	1.03	-0.53	0.27
SD	2.89	2.89	0.83	3.10	0.45
Max	26.46	4.46	3.24	3.72	0.96
Min	17.57	-4.43	0.23	-6.35	-0.67

SD, standard deviation; SEQ, spherical equivalent.

Infants and Toddlers

The open-field infant keratometer was then used by one experienced investigator to record images from 10 infants and toddlers. No quantitative analysis was performed, but a report on the subjective impressions of the instrument operator was obtained. The open-field design was reported to be much easier to use with infants and young children, and the instrument was felt to be more physically robust than the IK4. Interpretable images were obtained from all 10 subjects. There was some tendency for the child to be looking upward in the recorded images, suggesting that the operator may have been making eye contact with the child from above the horizontal plane.

SUBJECTIVE INTERPRETATION OF GRID ARRAY IMAGES

The grid array image, seen in the inset of Figure 7, center right, was found in all interpretable images and demonstrated that the coaxial illumination array could be used with infants to create an image for interpretation of higher-order aberrations. It was clear that the images could be further optimized, because smaller IRLEDs as used in the ring array could be used. In the prototype, the large IRLEDs were used because there was concern that not enough light would reflect off M3 to adequately illuminate the cornea.

DISCUSSION

The introduction of an open-field handheld keratometer is a novel contribution to the state of the art of keratometry, allowing for better social interaction of the infant and toddler and permitting binocular viewing of the child. The current design has not been

evaluated for clinical accuracy in infants and toddlers, but it has been shown to offer high testability, allowing 10 of 10 infants and toddlers to be studied and to have interpretable images obtained from all 10 subjects.

An important advance in keratometry that is offered by the present design is the elimination of the "black hole" in the center of the keratoscope, where the imaging lens is located on conventional keratometers. Conventional ring keratoscopes are unable to image the center portion of the cornea, because of the presence of the lens. The open-field design presented in this instrument uniquely incorporates a grid array at the corneal apex and demonstrates the potential for new methods of analysis that deviate from ring keratoscopy and allow for measurement of corneal power at the corneal apex, previously unobtainable from conventional ring keratoscopes incorporating an imaging lens with coaxial rings.

A significant design tradeoff occurred in the design of the open-field keratometer, and that tradeoff was a much shorter working distance of 25 mm for binocular viewing by the child. For a ring keratoscope to be placed close enough to the child's eye to permit evaluation of the corneal power at a radial distance of approximately 1.75 mm, and simultaneously keeping the ring small enough that it could be centered on the right eye of a child, it was necessary to limit the ring diameter to 50 mm. This limitation was a result of the necessity to keep the ring centered on the child's eye, and not extending past the typical child's nasal bridge and obscuring the vision of the left eye. To sample a radius of 1.75 mm of the typical cornea, the distance of this 50-mm ring is 40 mm, with a depth of focus of an additional 25 mm. Although this placed the faceplate of the keratometer quite close to the baby, because the child was viewing through windows and making eye contact with the examiner, it appears that the working distance is not inherently a detriment to testability.

However, as seen in the "Results" section, with the short working distance of 40 mm, and depth of focus of 25 mm, the accuracy of the instrument in adults for base curvature measurement was unacceptable (standard deviation, 3 D). Had the depth of focus been significantly smaller, the accuracy of the instrument would increase, but the testability would decrease (a consequence of needing to precisely position a handheld instrument before a wiggly infant or toddler). There is 38% difference between 40 mm and 25 mm, and while the telecentric lens did not introduce errors associated with this change in distance, the use of point sources of light did affect the size of the corneal reflected image.

LIMITATIONS INDUCED BY USING REAL OBJECTS AT NEAR DISTANCES

The use of real objects at near distances for keratometry results in unavoidable variation in image size with variation in vertex distance from the object to the cornea. This is best observed through inspection of Figure 11, which expands the ray diagram of Figure 1 to show the effect of varying the vertex distance on resultant image size. In Figure 11, at the top of the image, point source PS (such as the LEDs used in the open-field keratometer) gives off diverging rays of light, some of which strike the cornea. In Figure 11, two corneal positions are shown at vertex distances V1 and V2. When the instrument is held closer to the eye (as in V1), the vergence of the light striking the cornea is greater, and so the image distance is lesser, with larger resultant images size S1 compared to image S2 obtained at a larger vertex distance.

In the open-field keratometer, the ring radius is 25 mm, V1 is 25 mm, and V2 is 50 mm. When the vergence formula is applied to a mirror arising from a corneal radius of curvature of 7.54 mm (corresponding to a corneal refracting power of 44.7 D and corneal reflecting power of -265.3 D), a theoretical image ring radius of 3.28 mm is obtained for the closest vertex distance of 25 mm, and 1.75 mm for the greatest vertex distance of 40 mm, where sharp images would be expected to be obtained. This theoretical prediction of image size agrees with the empirical observations of Figure 10 and represents a 46% change in image size over the range of vertex distances expected to be encountered when the instrument is used in a handheld manner.

This variation in image size is much greater than that which was observed for keratometers with a greater vertex distance. For example, the IK4 has a ring radius of 90 mm, minimum vertex distance of 150 mm, and maximum vertex distance of 175 mm. For the same 7.54-mm radius cornea, the theoretical ring radii associated with these vertex distances are 2.21 mm and 1.90 mm, respectively, representing a 14% change in image size over the range of expected vertex distances. The greater vertex distance results in a smaller percent variation in image size, with corresponding increased accuracy.

OVERCOMING SHORT VERTEX DISTANCE LIMITATIONS

As seen in Figure 11, the variation in image size resulting from variation in vertex distance arises from real objects having divergent light rays exiting them, and those diverging rays having different vergence at different vertex distances. If the vergence of light coming from the object did not change with vertex distance, there would be no associated image size variation.

The error associated with a change in vertex distance decreases with increasing vertex distance, with the optimum vertex distance being infinity; if the object were infinitely far away, the increase in vertex distance of 25 mm would have no effect. While it is not possible to put a ring of point sources at infinity, it is possible to optically place them at infinity through the use of a collimating lens.

In the lower portion of Figure 11, there is a collimated light source shown as CS. A collimating lens is a lens placed its focal length away from a point source. The larger the diameter of the collimating lens, the greater the volume of space illuminated by that source, and the greater the variation in vertex distance that can be achieved without change in image size. For Figure 11, when a collimated light source is used as shown, if the same parameters are specified for the open-field keratometer (corneal radius of 7.54 mm, ring radius of 25 mm, V1 of 25 mm, and V2 of 50 mm), the size of the corneal image would be 2.26 mm, regardless of the vertex distance. If collimated light sources were to be used instead of point sources, the observed variation in image size would not occur with variation in vertex distance. If a telecentric lens were combined with collimated light sources, accuracy should be independent of vertex distance over the range of focus.

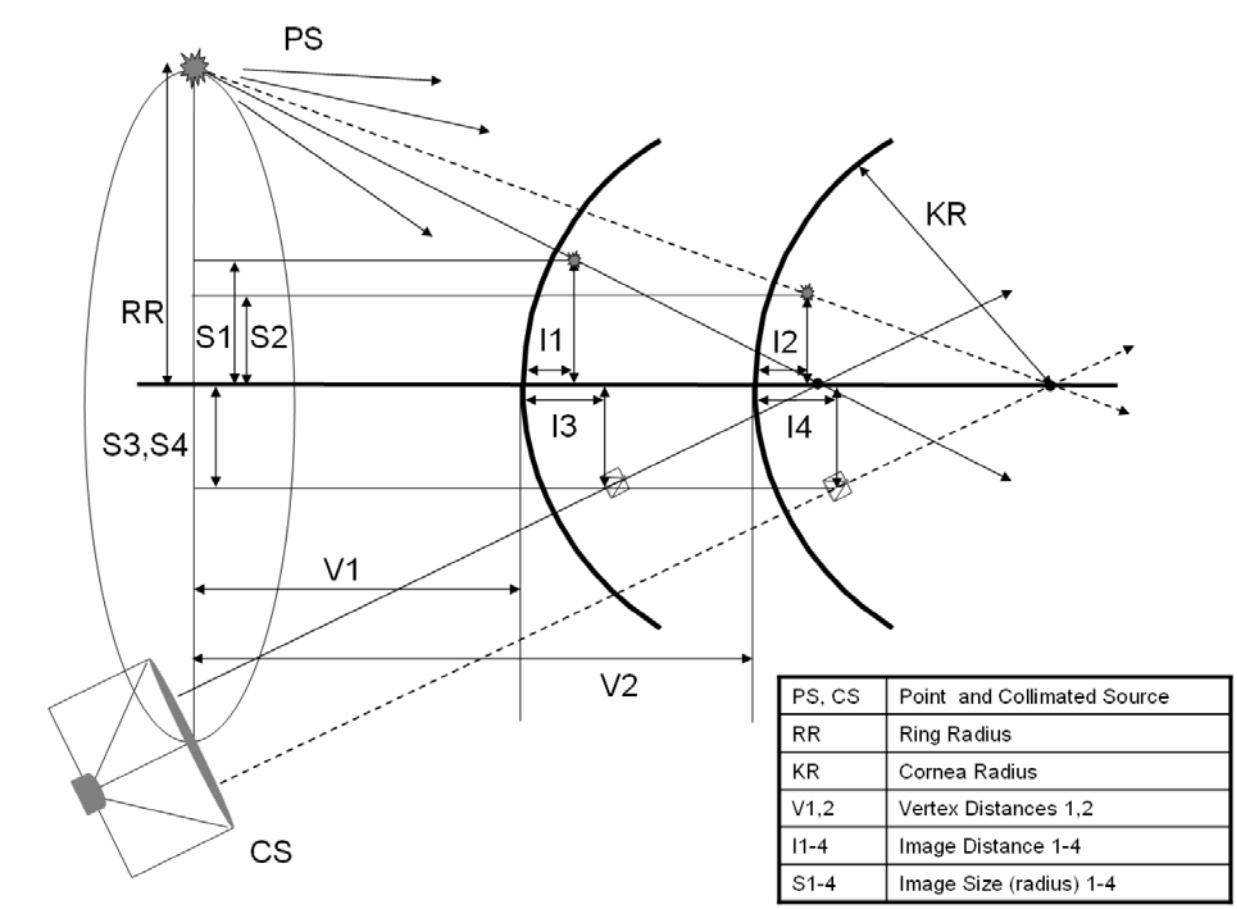

FIGURE 11

Point and collimated light sources in keratometer design. The point source of light PS emits light in all directions. Because the rays leaving the point source are not parallel, the vergence of the light striking the cornea varies with the distance from the light source to the cornea, resulting in a change in corneal image size with change in vertex distance, as seen with I1 being different in size than I2. This effect is not seen when collimated sources (CS) are used. The collimating lens allows parallel rays of light to exit across the area of the lens, and define a volume of space in which the cornea will be illuminated with rays of light having constant zero vergence. Within this volume of space corneal image size will not change with vertex distance, as seen by I3 being the same size as I4.

The disadvantage of using collimated light sources is that of complexity. LED light sources have a hemispheric lens incorporated in their construction that typically has a viewing angle to half intensity of 45º. If the LEDs are to be used with a collimating lens, it is necessary that the lens be sufficiently wide to create the corresponding depth of field provided by the telecentric imaging lens, with sufficient plus power to be close enough to the LED to capture light across the entire width of the lens. The result is that each point source (a single LED) becomes a projector (consisting of an enclosure, a LED, and a plus lens).

DEMONSTRATION OF CONCEPT: USE OF COLLIMATED LIGHT SOURCES FOR KERATOMETRY

Figure 12, left, shows a prototype ring keratometer (IK6) built to demonstrate the use of collimated light sources for the purposes of keratometry. In the device shown, 12 projectors were constructed, each incorporating an IR-LED and a 25-mm-diameter, 15 D plastic plus lens. The lens diameter allowed for a depth of focus with uniform illumination of 25 mm. The projectors were simultaneously aimed to the same point in space, at an angle with respect to the optical axis corresponding to that of the ring keratometer IK4, effectively having the same angle as a 90-mm radius ring at a vertex distance of 150 to 175 mm. This allowed direct comparison to the IK4 in terms of the effect of vertex distance.

This prototype was effective at demonstrating proof of concept, for the expected changes in magnification predicted for the IK4 were observed with variation in vertex distance, but were not seen with the IK6. The disadvantage of the IK6 that prevents it from being clinically useful is the lack of an open-field design. Figure 12, right, shows a front view of the device. It would be possible to

construct a coaxial camera mount with surrounding ring of collimated light projectors, and even incorporate a pair of beam splitters to permit open-field viewing of the child's eyes at a distance of 150 mm. However, including these projectors in the present instrument is not possible because of space limitations within the optical head of the open-field keratometer.

FIGURE 12

IK6, collimated mire prototype keratometer (left, rear; right, front), demonstrating use of collimated light sources to eliminate the effect of vertex distance image size changes. Each of the small projectors contain an infrared light-emitting diode that is positioned so the image of the LED source is placed at the posterior focal length of a 25-mm-diameter collimating lens. Collimated light exits from each of the 12 projectors to a common volume in space approximately 25 mm in diameter, within which the cornea can be imaged without variation in image size being associated with change in position. This provides a volume of space within which the telecentric imaging system will see a constant-sized image of a target, optically located at infinity.

FUTURE WORK

The open-field keratometer has demonstrated the potential to make keratometric measurements in toddlers and children using an instrument with a close (25-mm) working distance through the use of an open-field design. The depth of focus of 25 mm provided by the telecentric lens proves to be too great in relation to the working distance when used with IRLEDs as point sources in the ring. For the device to prove to have acceptable accuracy in the measurement of corneal base curvature, it will be necessary to place collimating lenses in association with each of the IRLEDs. The smaller the diameter of lens used, the greater the reduction in vertex distance variation, but with greater accuracy. Such modifications to the present open-field design will be required for the described device to be clinically usable. Incorporating such modifications in the present design, with additional consideration for including collimated sources for the central grid array, will represent the direction of future efforts of this work in progress.

ACKNOWLEDGMENTS

Funding/Support: This work is funded in part by the University of Arizona Pilot Grants Program; the Whitaker Foundation for Biomedical Research; grants EY11155, EY13153, and EYEY08893-12 from the National Eye Institute, National Institutes of Health; a challenge grant and center grant from Research to Prevent Blindness Inc; and a Walter E. and Lilly Disney Award for amblyopia research.

Financial Disclosures: None.

Conformity With Author Information: The University of Arizona Institutional Review Board approved this research. A properly executed consent form was obtained from each subject who participated in the research. The Declarations of Helsinki were followed.

Other Acknowledgments: I gratefully acknowledge David Guyton, MD, who instructed me in ophthalmic optics while I was a clinical fellow and continued to mentor me throughout my career; Jim Schwiegerling, PhD, who started as the student and in no time became the teacher; Candice E. Clifford-Donaldson, MPH, who assisted with data collection; and Velma Dobson, PhD, who taught me so much about the most important thing in experimental design: What question are you asking?

REFERENCES

1. Fulton AB, Dobson V, Salem, et al. Cycloplegic refractions in infants and young children. *Am J Ophthalmol* 1980;90:239-247.
2. Miller JM, Dobson V, Harvey EM, et al. Astigmatism and amblyopia among Native American children (AANAC): design and methods. *Ophthalmic Epidemiol* 2000;7:187-207.
3. Miller JM, Dobson V, Harvey EM, et al. Comparison of preschool vision screening methods in a population with a high prevalence of astigmatism. *Invest Ophthalmol Vis Sci* 2001;42:917-924.
4. Rowsey JJ, Reynolds AE, Brown R. Corneal topography-corneascope. *Arch Ophthalmol* 1981;99:1093-1100.
5. Guyton DL, West CE, Miller JM, et al. *Ophthalmic Optics and Clinical Refraction*. Baltimore: Prism Press; 1997.
6. Placido A. Novo instrumento de esploracro da cornea: astigmatoscio explorado. *Periodica Oftalmol Practica Lisb* 1880;5:27-30.
7. Southall JPC, ed. *Helmholtz's Treatise on Physiological Optics* [translated from the third German edition], vol 1. Rochester, NY: Optical Society of America; 1924:14.
8. Javal L, Schiötz H. Un opthalmomètre pratique. *Ann Oculist* 1881;86:5-21.
9. Miller JM, Schwiegerling J. A videokeratoscope using a distorted checkerboard target. In: *Vision Science and Its Applications*. Washington, DC: Optical Society of America; 1998:227-230. OSA Technical Digest Series, vol 1.
10. Harvey EM, Miller JM, Dobson VD. Reproducibility of corneal astigmatism measurements with a hand-held keratometer in preschool children. *Br J Ophthalmol* 1995;79:983-990.
11. Dobson V, Miller JM, Harvey EM. Corneal and refractive astigmatism in a sample of 3- to 5-year-olds with a high prevalence of astigmatism. *Optom Vis Sci* 1999;76:855-860.
12. Mandell RB. Reflection point ophthalmometry: a method to measure corneal contour. *Am J Optom Arch Am Acad Optom* 1966;39:513-537.
13. Gullstrand A. Photographic-ophthalmometric and clinical investigations of corneal refraction part 1. *Am J Optom Arch Am Acad Optom* 1966;43:143 [first appearing in 1893, translated in 1964 by William M. Ludlam, with Appendix by Sydney Wittenberg].
14. Miller JM, Mellinger M, Greivenkamp J, et al. Video remote keratometer for the screening of corneal astigmatism. In: *Ophthalmic and Visual Optics/Noninvasive Assessment of the Visual System.* Washington, DC: Optical Society of America; 1993:150-153. OSA Technical Digest Series, vol 3.
15. Mandell RB. Corneal contour of the human infant. *Arch Ophthalmol* 1967;77:345-348.
16. Howland HC, Sayles N. Photokeratometric and photorefractive measurements of astigmatism in infants and young children. *Vision Res* 1985;25:73-81.
17. Klyce SD. Computer-assisted corneal topography: high-resolution graphic presentation and analysis of keratoscopy. *Invest Ophthalmol Vis Sci* 1984;25:1426-1435.
18. Fowler CW, Dave TN. Review of past and present techniques of measuring corneal topography. *Ophthalmic Physiol Opt* 1994;14:49-58.
19. Klein SA. Uniqueness of corneal shape from Placido ring images. In: *Ophthalmic and Visual Optics/Noninvasive Assessment of the Visual System*. Washington, DC: Optical Society of America; 1996:204-207. OSA Technical Digest Series, vol 1.
20. Gills J, Sanders DR, Thornton SP, et al. *Corneal Topography: The State of the Art.* Thorofare, NJ: Slack Inc; 2005.
21. Schwiegerling J. The optics of wavefront technology. In: Tasman W, Jaeger EA, eds. *Duane's Clinical Ophthalmology*. Philadelphia, PA: Lippincott; 2004.
22. Schwiegerling J, Greivenkamp JE, Miller JM. Zernike polynomial representations of videokeratoscope height data. In: *Vision Science and Its Applications*. Washington, DC: Optical Society of America; 1995:192. OSA Technical Digest Series, vol 1.
23. Schwiegerling J, Greivenkamp JE, Miller JM, Snyder RW, Palmer ML. Optical modeling of radial keratotomy incision patterns. *Am J Ophthalmol* 1996;12:808-817.
24. Prakash G, Sharma N, Chowdhary V, et al. Association between amblyopia and higher-order aberrations. *J Cataract Refract Surg* 2007;33:901-904.
25. Kirwan C, O'Keefe M. Association between amblyopia and HOAs . *J Cataract Refract Surg* 2007;33:1833.
26. Press WH, Flannery BP, Teukolsky SA, Vetterling WT. *Numerical Recipes in C: The Art of Scientific Computing.* New York, NY: Cambridge University Press; 1992.
27. Miller JM, Mellinger M, Greivenkamp J, et al. Videographic Hirschberg measurement of simulated strabismic deviations. *Invest Ophthalmol Vis Sci* 1993;34:3220-3229.
28. Hall HL, Miller JM, Greivenkamp JE. Binocular pupil brightness changes in the presence of strabismus: predictions from computer modeling. In: *Vision Science and Its Applications*. Washington, DC: Optical Society of America; 1995:92-95. OSA Technical Digest Series, vol 1.